A Robust Maximum Power Point Tracking Control Strategy for Doubly-Fed Induction Generator Wind Turbines Using Advanced Sliding Mode Control Under Variable Wind Conditions.

Hichem ITOUCHENE[1*], Fayssal AMRANE[2], Zoubir BOUDRIES[1]

[1] Laboratoire de Technologie Industrielle et de l'Information (LTII), Faculté de Technologie, Université de Bejaia, 06000 Bejaia, Algérie, zoubir.boudries@univ-bejaia.dz / +213 560 692 724

[2] LAS Research Laboratory, Department of Electrical Engineering, Ferhat ABBAS Setif-1 University, 19000 Setif, Algeria. amrane_fayssal@univ-setif.dz / amranefayssal@gmail.com /+213 658 267 565

[*] Corresponding author, e-mail: hichem.itouchene@univ-bejaia.dz / itouchene.hichem21@gmail.com / +213 561 917 554

Abstract- *Wind energy plays a pivotal role in the transition to sustainable energy sources. This paper presents a robust control strategy, the Variable Gain Super Twisting Sliding Mode Control (VGSTA-SMC), applied at the maximum power point tracking (MPPT) level. VGSTA-SMC is designed to precisely locate the MPPT, maximizing wind energy extraction while enhancing tracking performance and system stability. The primary objective is to improve the performance of Doubly Fed Induction Generator (DFIG) wind turbines under sudden wind speed variations by reducing the chattering phenomenon, managing external disturbances, and addressing slow response issues. The effectiveness of the proposed control strategy is verified by comparing it with Third-Order Sliding Mode Control (TO-SMC) and Proportional-Integral (PI) control. Simulation results using MATLAB/Simulink demonstrate that the proposed method enhances resilience to wind speed fluctuations and system uncertainties, ensuring smooth and efficient operation. By overcoming the limitations of conventional control methods, this strategy supports the broader adoption of wind energy systems. The study underscores the potential of advanced control techniques in optimizing renewable energy systems.*

Keywords: Wind Energy, DFIG, MPPT, Sliding Mode Control, PI Controller, Chattering Phenomenon.

1. Introduction

Across the world, wind is now one of the most cost competitive energy sources [1]. A significant global challenge is emerging today in the realm of energy resources. It's essential to recognize that wind power capacity may fluctuate annually, influenced by factors such as government policies, technological progress, and investment in the wind energy sector [2-3]. *Figure 1* illustrates the global wind power capacity growth from 2001 to 2020. It doubled from 24 GW to 59 GW by 2005, reached about 198 GW in 2010, and grew to over 433 GW by 2015. By 2020, it surpassed 792 GW, highlighting the global shift toward sustainable energy sources [4-5].

The International Energy Agency (IEA) projects renewable energy capacity growth under three scenarios (see *Figure 2*): reference (3,500 GW by 2050), moderate (3,000 GW by 2030 and 7,300 GW by 2050), and advanced (2,500 GW by 2030 and 11,000 GW by 2050), with the Net Zero by 2050 scenario showing the strongest growth [6]. This surge reflects rising workforce

demand, with about 600,000 skilled workers needed for global wind projects by 2027. *Table 1* from GWEC outlines expected capacity additions and training needs for construction, installation, and maintenance across ten countries and globally from 2023 to 2027 [7].

Electrical energy generation typically involves converting mechanical energy into electrical energy using generators [8]. The doubly-fed induction generator (DFIG) introduced in 1899, brought significant advancements to this field [9]. In wind energy conversion systems (WECS), DFIGs feature a distinct setup with the stator connected to the grid and the rotor linked via back-to-back converters [10]. A key benefit of DFIGs is that they reduce the load on power electronic equipment to just 20% to 30% of total system power [11], as noted by [12-13]. Nevertheless, DFIGs require complex control due to their operation at both sub- and super-synchronous speeds, demanding accurate regulation of rotor voltages [12-15].

Sliding mode control (SMC) offers an effective alternative to the conventional proportional-integral (PI) control method [16]. The latter is influenced by changes in machine parameters [17,18], leading to performance degradation. SMC excels in addressing this issue, offering robustness to parameter variations. However, one drawback of SMC is the phenomenon known as chattering (refer to *Figure 3),* which can introduce high-frequency oscillations into the control signal. *Figure 4* illustrates the block diagram of a SMC system.

The MPPT strategy has been a cornerstone of research in renewable energy initially developed for solar energy in the 1980s and successfully applied to wind energy as well. To optimize energy production, a range of algorithms has emerged [19], representing the ongoing evolution of strategies for maximizing power extraction from renewable sources. Typically, in WECS, MPPT techniques are utilized to harvest wind energy at its maximum potential [20]. Researchers have devised diverse control strategies centered around MPPT in WECS, including P&O [20], Artificial Neural Network Controller [18,21], adaptive neuro-fuzzy [22], fractional-order PI controller (FOPI) technique [23], adaptive controller [24], and a hybrid approach involving Backstepping and LQR control [25]. Efforts have also been directed towards the rotary side converter, enhancing system performance through varied control methods. In [26], a robust control strategy for a fractional-order DFIG model in variable-speed WT is proposed. It employs a fractional-order Backstepping sliding mode controller to manage generator speed and currents while mitigating nonlinearities, disturbances, and uncertainties. A fractional-order-SM disturbance observer estimates disturbances, and Ant Colony Optimization tunes the controller. Simulations

show the method outperforms conventional Backstepping-SMC in robustness and power optimization. Additionally, ref. [27] introduces an adaptive fixed-time control strategy for MPPT in DFIG-based WES. The approach includes a fixed-time observer that estimates torque without wind sensors, allowing real-time optimal speed control. An adaptive sliding SMC ensures accurate speed tracking, maintaining robustness without prior disturbance knowledge. Stability and convergence are verified using Lyapunov analysis. In [28], a novel MPPT controller for DFIG-based WECS combines sliding mode control with state and disturbance observers to achieve robust, fixed-time stability. It regulates stator reactive power and rotor speed, using a disturbance observer to manage uncertainties without requiring their bounds. The method avoids chattering and ensures stability via Lyapunov analysis, outperforming conventional finite-time approaches. However, it may face limitations due to the use of discontinuous Lyapunov functions, potentially affecting stability precision. Other innovative MPPT strategies include the MPPT-Fuzzy controller architecture [29] and the voltage-power (U-P) curve-based algorithm [30], developed for small-scale turbines to improve control quality and reduce measurement dependency. This study, in contrast, applies the nonlinear VGSTA-SMC method to MPPT and evaluates its performance against the traditional PI controller.

This study presents an MPPT control strategy for WES using the VGSTA control method, aiming to overcome the limitations of traditional controllers like PI and TO-SMC, especially under variable wind conditions. The VGSTA-SMC controller is designed to enhance performance by improving response time, reducing overshoot, and increasing power quality. Key improvements include better control of generated power, electromagnetic torque, grid-side currents, and reduced Total Harmonic Distortion (THD). Overall, it seeks to maximize power extraction and improve system durability under fluctuating wind speeds.

The main contributions of this paper are:

1- *Proposing a novel VGSTA-SMC-based MPPT strategy for DFIG wind turbines, enabling efficient power extraction under varying wind conditions and enhancing energy conversion efficiency.*
2- *Improved response time and minimized errors compared to traditional controls, resulting in faster adaptation to changes in wind speed.*
3- *Applying the proposed control at the MPPT level to boost DFIG wind turbine performance, ensuring faster convergence and system stability.*

4- *Enhancing of the DFIG's ability to handle uncertainties and disturbances in the wind turbine system.*
5- *Minimizing chattering by dynamically tuning gain parameters based on system states, unlike traditional SMC methods with fixed gains.*

The remaining part of this paper is organized as follows: Section 2 presents a detailed modeling of the WECS. Initially, the DFIG model and the mathematical model of the wind turbine are introduced. This section also covers MPPT with and without wind speed control, and separately models the applied *PI* controller, *TO-SMC*, and *VGSTA-SMC* controllers for MPPT, supported by illustrative diagrams. Section 3 provides analysis of performance indices to ensure the effectiveness of the proposed control strategy, which is observed through simulation results presented in section 4. Section 5 concludes the paper, presenting conclusions and future work for continuing research in this topic. Finally, the reported work is concluded.

2. Wind energy conversion system modeling

Modern wind turbines employ an advanced system to convert wind's kinetic energy into electrical energy, as shown in *Figure 5*. The wind's motion turns the blades, generating mechanical energy. This rotational energy is transferred through a shaft to a generator, where it is transformed into electrical energy via electromagnetic induction [2,8].

2.1. Modeling of DFIG

After applying the Park transform, we obtain the rotor and stator voltages for the DFIG, additionally, the flux equations, as follows [25,31-34]:

$$\begin{cases} V_{sd} = R_s I_{sd} + \dfrac{d\phi_{sd}}{dt} - \omega_s \phi_{sq} \\ V_{rd} = R_r I_{rd} + \dfrac{d\phi_{rd}}{dt} - \left(\omega_s - \omega_r\right)\phi_{rq} \\ V_{sq} = R_s I_{sq} + \dfrac{d\phi_{sq}}{dt} + \omega_s \phi_{sd} \\ V_{rq} = R_r I_{rq} + \dfrac{d\phi_{rq}}{dt} - \left(\omega_s - \omega_r\right)\phi_{rd} \end{cases} \tag{1}$$

$$\begin{cases} \phi_{sd} = L_s.I_{sd} + M.I_{rd} \\ \phi_{rd} = L_r.I_{rd} + M.I_{sd} \\ \phi_{sq} = L_s.I_{sq} + M.I_{rq} \\ \phi_{rq} = L_r.I_{rq} + M.I_{sq} \end{cases} \tag{2}$$

The electromagnetic torque and the stator active/reactive powers are given by

$$T_{em} = (3/2)\left[\frac{P.M}{L_s}\left(\phi_{sq}.I_{rd} - \phi_{sd}.I_{rq}\right)\right] \quad (3)$$

$$T_{em} - T_g = J\frac{d\Omega_g}{dt} + f_r\Omega_g \quad (4)$$

$$\begin{cases} P_s = (3/2)\left[V_{sd}.I_{sd} + V_{sq}.I_{sq}\right] \\ Q_s = (3/2)\left[V_{sq}.I_{sd} - V_{sd}.I_{sq}\right] \end{cases} \quad (5)$$

2.2. Wind Turbine Modeling

The wind is a stochastic variable [35], characterized by its direction and speed, which are influenced by factors such as location and climate conditions [36]. The expressions for the input power, mechanical power, and torque of the WT are given as follows [37, 38]:

$$P_v = \frac{1}{2}\rho.\pi.R^2.v^3 \quad (6)$$

$$P_t = P_v.C_p = \frac{1}{2}\rho.\pi.R^2.v^3.C_p(\lambda,\beta) \quad (7)$$

$$T_t = \frac{P_t}{\Omega_t} \quad (8)$$

The power coefficient C_p can be described as [38]:

$$C_p(\lambda,\beta) = 0.5176\left(\frac{116}{\lambda_i} - 0.4\beta - 5\right)e^{-\frac{21}{\lambda_i}} + 0.0068\lambda \quad (9)$$

Where:

$$\lambda = \frac{R.\Omega_t}{v}, \frac{1}{\lambda_i} = \frac{1}{\lambda + 0.08\beta} - \frac{0.035}{\beta^3 + 1}$$

Using the previous equations, the WT diagram can be simplified, as shown in *Figure 6*.

2.3 . MPPT modeling

MPPT is a control strategy that ensures that a WT operates at its maximum power point (MPP) under varying wind conditions. This is important because the MPP is the point where the wind turbine generates the most power for a given wind speed [39]. There are two main types of MPPT strategies:

2.3.1. MPPT strategy without wind speed control

To maximize wind energy extraction, the rotational speed of the turbine must be continually adjusted in response to wind speed variations [13]. The underlying principle of this control strategy

is to maintain a turbine rotational speed that ensures an optimal speed ratio $\lambda=\lambda_{opt}$. The block diagram in *Figure7* illustrates the principle of MPPT control for the wind turbine without rotation speed feedback. The electromagnetic torque reference is determined based on an estimated wind speed, which is derived from the control of mechanical rotational speed [39, 40]. This value, expressed by equation (10), can be inferred from equations (11), (12), and (13).

$$\Omega_t = \frac{\Omega_g}{G} \tag{10}$$

$$\hat{v} = \frac{R.\Omega_t}{\lambda} \tag{11}$$

$$T_t = \frac{1}{2.\Omega_t}\rho.\pi.R^2.\hat{v}^3.C_{p-\max} \tag{12}$$

$$T_g^{ref} = \frac{T_t}{G} \tag{13}$$

2.3.2. MPPT strategy with wind speed control

The MPPT method aims to improve the efficiency of the WECS by maximizing wind power extraction through rotor speed control. This is achieved by adjusting the electromagnetic torque to maintain the desired rotor speed, as specified by the MPPT strategy. In this control scheme, the WT's torque is considered a disturbance and is compensated accordingly [12, 41]. A fundamental diagram of this control approach, incorporating wind speed regulation, is derived based on following equations.

$$\Omega_g^{ref} = G.\Omega_t^{ref} \tag{14}$$

$$\Omega_t^{ref} = \frac{\lambda_{opt}.C_{p-\max}v}{R} \tag{15}$$

To ensure optimal MPPT system performance, rotor speed is controlled using three main techniques: PI, TO-SMC, and VGSTA-SMC. Each method offers a unique strategy for enhancing tracking efficiency. The controller gains depend largely on the generator's internal mechanical characteristics [35, 42–43]. The linear PI controller is illustrated in *Figure 8*, while the nonlinear TO-SMC and VGSTA-SMC controllers are shown in *Figures 9 and 10*, respectively. Under ideal conditions, the electromagnetic torque matches its reference value, independent of the generated power. This reference torque is determined by the speed controller to ensure the rotor speed tracks its desired value.

2.3.2.1 MPPT Algorithm based on PI-Controller

The reference electromagnetic torque is provided as follows [20]:

$$T_{em\_PI} = PI\left(e\left(\Omega_g\right)\right) = PI\left(\Omega_g^{ref} - \Omega_g\right) \tag{16}$$

Where:

$$\Omega_g^{ref} = G.\Omega_t^{ref} \tag{17}$$

$$\Omega_{\mathrm{t}}^{\mathrm{ref}} = \frac{\lambda_{opt}.C_{p-\max}v}{R} \tag{18}$$

The standard form of the *PI* controller transfer function (TF) is represented in the Laplace domain in equation (5). This equation describes how the output of the *PI* controller depends on the error signal and it's integral over time [44-45].

$$TF\left(PI\right) = K_P + \frac{K_i}{S} = \frac{\left(K_P.S + K_i\right)}{S} \tag{19}$$

Where: K_P, K_i: are the proportional and integral gains, respectively, and *S* is the Laplace variable representing the frequency domain.

2.3.2.2 MPPT Algorithm based on TO-SM Controller

The third-order sliding mode controller (*TO-SMC*) is a robust and powerful control approach widely recognized for its effectiveness in system regulation and the simplicity of its algorithm. It serves as an alternative to traditional linear and nonlinear control methods, addressing the primary limitations associated with conventional *SMC*, particularly the chattering phenomenon. The *TO-SMC* control methodology is defined by the following equations [46]:

$$T_{em\_TOSMC} = M_1\sqrt{\left|e\left(\Omega_g\right)\right|}.sign\left(e\left(\Omega_g\right)\right) + M_2\int sign\left(e\left(\Omega_g\right)\right)\mathrm{dt} + M_3 sign\left(e\left(\Omega_g\right)\right) \tag{20}$$

Where: $\mathrm{e}\left(\Omega_{\mathrm{g}}\right) = \Omega_g^{ref} - \Omega_g$

The tuning constants M_1, M_2, and M_3 are used to improve the performance of the *TO-SMC* method. The *TO-SMC* controller scheme is presented in *Figure 9*.

2.3.2.3 MPPT Algorithm based on VGSTA-SM Controller

2.3.2.3.1 Problem Statement

Let us examine a linear time-invariant system subject to a nonlinear perturbation

$$\dot{x} = Ax + B\left(u + \xi\left(x,t\right)\right) \tag{21}$$

The system's internal state and control input are represented by vectors $x \in R^n$ and $u \in R^m$, respectively. Assuming *B* has full rank, *(A, B)* is controllable, and the disturbance function is bounded, a linear state transformation can be applied.

$$\begin{pmatrix} h_1 \\ h_2 \end{pmatrix} = Tx, T = \begin{bmatrix} B^{\perp} \\ B^{+} \end{bmatrix}, B^{+} = \left(B^T B\right)^{-1} B^T, B^{\perp} B = 0 \tag{22}$$

The system described in equation (21) is in the regular form.

$$\begin{aligned} \dot{h}_1 &= A_{11} h_1 + A_{12} h_2 \\ \dot{h}_2 &= A_{21} h_1 + A_{22} h_2 + u + \xi\left(h_1, h_2, t\right) \end{aligned} \tag{23}$$

Where $h_1 \in R^{(n-m)}$ and $h_2 \in R^m$. The system's structure allows us to focus exclusively on the single-input scenario *(m=1)* without loss of generality, as the results can be easily extended to the multi-input case [46]. The sliding surface is defined accordingly:

$$e = h_2 - \alpha h_1 = 0 \tag{24}$$

As a result, when the motion is restricted to the manifold, the simplified order model accurately represents the system.

$$\dot{h}_1 = \left(A_{11} + A_{12}\alpha\right) h_1 \tag{25}$$

The desired performance can be achieved. As the pair (A_{11},A_{12}) is controllable, the matrix α can be designed using any suitable linear control design technique for system (25). Using (h_1,e) as state variables and applying the controller

$$u = -\left(A_{21} + A_{22}\alpha - \alpha\left(A_{11} + A_{12}\alpha\right)\right) h_1 - \left(A_{22} - \alpha A_{12}\right) e + v \tag{26}$$

The system (23) is expressed in the following form

$$\dot{h}_1 = \left(A_{11} + A_{12}\alpha\right) h_1 + A_{12} e \tag{27}$$

$$\dot{e} = v + \tilde{\xi}\left(h_1, e + \alpha h_1, t\right) \tag{28}$$

When the perturbation is constrained by a known function $\vartheta\left(x\right)$ a 1st-SM can be enforced by a variable-gain controller

$$\left|\xi\left(x,t\right)\right| \le \vartheta\left(x\right) \tag{29}$$

$$v = -\left(\vartheta\left(x\right) + \vartheta_0\right) sign\left(e\right) \tag{30}$$

With $\vartheta_0 > 0$, the primary limitation of this controller is the chattering effect, which becomes more pronounced as the uncertainty bound $\vartheta(x)$ increases. To address this issue, a Lyapunov-based design for the STA is proposed, incorporating linear terms and variable gains to mitigate the drawbacks of the conventional STA. These enhancements are essential, as the geometric and homogeneity-based proofs of the standard STA cannot accommodate such modifications [46]. The control law of the VGSTA can be expressed as:

$$T_{em\_VGSTA} = -\alpha_1(t,X) * F_1\left(e(\Omega_g)\right) - \int_0^t \alpha_2(t,X) * F_2\left(e(\Omega_g)\right) dt \tag{31}$$

Where:

$$F_1\left(e(\Omega_g)\right) = \left|e\left(\Omega_g\right)\right|^{0.5} sign\left(e(\Omega_g)\right) + \alpha_3 e(\Omega_g) \tag{32}$$

$$F_2\left(e(\Omega_g)\right) = \frac{1}{2} sign\left(e(\Omega_g)\right) + \frac{3}{2}\left|e\left(\Omega_g\right)\right|^{0.5} sign\left(e(\Omega_g)\right) + \alpha_3^2 e(\Omega_g),\ \ \alpha_3 > 0 \tag{33}$$

When the gain $\alpha_3 = 0$ and α_1, α_2 are constant, the control algorithm simplifies to the classical STSMC, ensuring finite-time convergence and robustness against bounded disturbances. Introducing $\alpha_3 > 0$ allows the algorithm to handle linearly growing perturbations with respect to the sliding variable, while variable gains α_1 and α_2 enhance robustness against state-dependent disturbances, reduce chattering, and maintain system stability [46, 47-48]. Such adaptability is particularly valuable in managing uncertainties from factors like wind speed variations, turbulence, and changes in generator parameters, can be expressed as follows:

$$\tilde{\varepsilon}\left(h_1, e+\alpha h_1, t\right) = \underbrace{\left[\tilde{\varepsilon}\left(h_1, e+\alpha h_1, t\right) - \tilde{\varepsilon}\left(h_1, \alpha h_1, t\right)\right]}_{g_1(h_1,e,t)} + \underbrace{\tilde{\varepsilon}\left(h_1, \alpha h_1, t\right)}_{g_2(h_1,t)} \tag{34}$$

Where:

$$\begin{aligned} &\left|g_1\left(h_1,e,t\right)\right| \le \vartheta_1(t,x)\left|W_1(e)\right|, \text{ with } \vartheta_1(t,x) \ge 0 \\ &\left|\frac{d}{dt} g_2\left(h_1,t\right)\right| \le \vartheta_2(t,x)\left|W_2(e)\right|, \text{ with } \vartheta_2(t,x) \ge 0 \end{aligned} \tag{35}$$

With: $\vartheta_2(t,x)$ and $\vartheta_1(t,x)$, are continuous and well-defined functions.

Where $g_1(h_1,e,t)=0$, under the condition $e=0$ assumption (A3) implies that the uncertainty or disturbance $\xi(x,t)$ remains bounded almost everywhere. The system described by equation (28), governed by the VGSTA as shown in equation (31), can be formulated as:

$$\begin{aligned}\dot{h}_1 &= \left(A_{11} + A_{12}\alpha\right)h_1 + A_{12}e \\ \dot{e} &= -\alpha_1(t,x)W_1(e) + h + g_1\left(h_1, e, t\right) \\ \dot{h}_0 &= -\alpha_2(t,x)W_2(e) + \frac{d}{dt}g_2\left(h_1, t\right)\end{aligned} \tag{36}$$

The algorithm is outlined in the theorem below:

Theorem. Let $\vartheta_1(\mathrm{t},\mathrm{x}) \geq 0, \vartheta_2(\mathrm{t},\mathrm{x}) \geq 0$ be continuous functions for which the inequalities (35) hold. Then, for any initial condition $\left(h_1(0), e(0), h_0(0)\right)$ the sliding surface *e=0,* will be reached in finite time, provided that the variable gains are chosen as specified in [49].

$$\begin{aligned}\alpha_1(t,x) &= \delta + \frac{1}{\beta}\left(\frac{1}{4\aleph}\left(2\aleph\vartheta_1 + \vartheta_2\right)^2 + +2\aleph\vartheta_2 + \aleph + \left(2\aleph + \vartheta_1\right)\left(\beta + 4\aleph^2\right)\right) \\ \alpha_2(t,x) &= \beta + 4\aleph^2 + 2\aleph h_1(t,x)\end{aligned} \tag{37}$$

2.3.2.3.2 Lyapunov Stability Analysis.

The time required to reach the sliding surface can be approximated by the following:

$$T = \frac{2}{\gamma_2}\ln\left(\frac{\gamma_2}{\gamma_1}V^{0.5}\left(e(0), h_0(0)\right) + 1\right) \tag{38}$$

Where $\beta > 0, \aleph > 0, \gamma > 0$, are arbitrary positive constants, $V\left(e, h_0\right) = \xi^T P\xi$, with:

$$\xi^T = \left[\,|e|^{0.5}\ sign(e) + \alpha_3 e, h_0\right] \text{ and } \gamma_1 = \frac{\aleph\lambda_{\min}^{0.5}\{P\}}{\lambda_{\max}\{P\}}, \gamma_2 = \frac{2\aleph\alpha_3}{\lambda_{\max}\{P\}}$$

Proof of Theorem: The proof of *Theorem 1* will be conducted using a strict Lyapunov function for the subsystem of equation (36). We will demonstrate that the quadratic form

$$V\left(e, h_0\right) = \xi^T P\xi \tag{39}$$

Where

$$\xi^T = \left[\,|e|^{0.5}\ sign(e) + \alpha_3 e, h_0\right] \tag{40}$$

$$P = \begin{bmatrix} P_1 & P_3 \\ P_3 & P_2 \end{bmatrix} = \begin{bmatrix} \beta + 4\aleph^2, & -2\aleph \\ -2\aleph & 1 \end{bmatrix} \tag{41}$$

For any positive constants $\beta > 0$, and $\aleph > 0$ the function serves as a Lyapunov function for the subsystem $\left(e, h_0\right)$ in equation (36), ensuring finite-time convergence. Function (39) is positive definite, continuous, and differentiable except on $S = \left\{\left(e, h_0\right) \in R^2 \mid e = 0\right\}$. The inequalities in

equation (35) can be expressed using bounded functions $g_1(h_1,e,t)=\propto_1(t,x)W_1(e)$ and $\frac{d}{dt}g_2(h_1,t)=\propto_2(t,x)W_2(e)$ for some functions $|\propto_1(t,x)|\le \vartheta_1(\mathrm{t,x})$ and $|\propto_2(t,x)|\le \vartheta_2(\mathrm{t,x})$ these relate to $W_1(e)$, and $W_2(e)$. By noting that $W_2(e)=W_1'W_1(e)$, these properties can be used to prove the desired results.

$$\begin{aligned}\dot{\xi}&=\begin{bmatrix}W_1'(e)\{-\alpha_1(t,x)W_1(e)+h_0+g_1(x,t)\}\\ -\alpha_2(t,x)W_2(e)+\frac{d}{dt}g_2(x,t)\end{bmatrix}\\ &=W_1'(e)\begin{bmatrix}-(\alpha_1(t,x)-\propto_1(t,x)), & 1\\ -(\alpha_2(t,x)-\propto_2(t,x)) & 0\end{bmatrix}\xi=W_1'(e)A(t,x)\xi\end{aligned}\tag{42}$$

For each point R^2 , S where this derivative exists, the derivative of $V(x)$ can similarly be computed as follows:

$$\dot{V}(e,h_0)=W_1'(e)\xi^T\left(A^T(t,x)P+P\,A(t,x)\right)\xi=-W_1'(e)\xi^TQ(t,x)\xi\tag{43}$$

$$Q(t,x)=\begin{bmatrix}2(\alpha_1(t,x)-\propto_1)P_1+2(\alpha_2(t,x)-\propto_2)P_3 & \text{å}\\ (\alpha_1(t,x)-\propto_1)P_3+(\alpha_2(t,x)-\propto_2)P_2-P_1, & -2P_3\end{bmatrix}\tag{44}$$

Using ⋆ to denote symmetric elements, by choosing *P* as defined in equation (41) and the gains as specified in (equation 37), we obtain

$$\begin{aligned}Q-2\aleph I&=\begin{bmatrix}2\beta\alpha_1+4\aleph(2\aleph\alpha_1-\alpha_2)-2(\beta+4\aleph^2)\propto_1+4\aleph\propto_2-2\aleph & \text{å}\\ \alpha_2-2\aleph\alpha_1-(\beta+4\aleph^2)+2\aleph\propto_1-\propto_2, & 2\aleph\end{bmatrix}\\ &=\begin{bmatrix}2\beta\alpha_1-(\beta+4\aleph^2)(4\aleph+2\propto_1)+4\aleph\propto_2-2\aleph & \text{å}\\ 2\aleph\propto_1-\propto_2, & 2\aleph\end{bmatrix}\end{aligned}\tag{45}$$

This is positive definite for all possible values of *(t,x)*, demonstrating that

$$\dot{V}=-W_1'(e)\xi^TQ(t,x)\xi\le-2\aleph W_1'(e)\xi^T\xi=-2\aleph\left(\frac{1}{2|e|^{0.5}}+\alpha_3\right)\xi^T\xi\tag{46}$$

Since, $\lambda_{\min}\{P\}\left\|\xi_2^2\right\|\le\xi^TP\xi\le\lambda_{\max}\{P\}\left\|\xi_2^2\right\|$

Where:

$$\left\|\xi_2^2\right\|=\xi_1^2+\xi_2^2=|e|+2\alpha_3|e|^{\frac{3}{2}}+\alpha_3^2e^2+h_0^2\tag{47}$$

$$\left|\xi_1\right| \le \left\|\xi_2\right\| \le \frac{V^{0.5}\left(e,h_0\right)}{\lambda_{\min}^{0.5}\left\{P\right\}} \tag{48}$$

$$\dot{V} \le -\gamma_1 V^{0.5}\left(e,h_0\right) - \gamma_2 V\left(e,h_0\right) \tag{49}$$

$$\gamma_1 = \frac{\aleph \lambda_{\min}^{0.5}\left\{P\right\}}{\lambda_{\max}\left\{P\right\}}, \gamma_2 = \frac{2\aleph \alpha_3}{\lambda_{\max}\left\{P\right\}} \tag{50}$$

Observe that the trajectories cannot remain within the set $S = \left\{\left(e,h_0\right) \in R^2 \mid e = 0\right\}$ Consequently; *V* behaves as a continuously decreasing function, allowing us to deduce that the equilibrium point $\left(e,h_0\right) = 0$ is achieved in finite time from any initial condition. Given that the solution of the differential equation

$$\dot{V} = -\gamma_1 V^{0.5} - \gamma_2 V, V\left(0\right) \ge 0 \tag{51}$$

$$V\left(t\right) = \exp\left(-\gamma_2 t\right)\left[V\left(0\right)^{0.5} + \frac{\gamma_1}{\gamma_2}\left(1 - \exp\left(\frac{\gamma_2}{2}t\right)\right)\right]^2 \tag{52}$$

It follows that $\left(e\left(t\right), h_0\left(t\right)\right)$converge to zero in finite time, reaching this value no later than the time specified in equation (38). This concludes the proof of ***Theorem.***

3. Analysis of performance indices

The controller's performance is evaluated using four criteria: Integral of Absolute Error (*IAE*), Integral of Squared Error (*ISE*), Integral Time Absolute Error (*ITAE*), and Integral Time Square Error (*ITSE*). These metrics provide a quantitative evaluation of the controller's performance [33, 50].

$$\mathrm{IAE} = \int_0^t \left|\mathrm{e}\left(\mathrm{t}\right)\right| \mathrm{dt}, \tag{53}$$

$$\mathrm{ITAE} = \int_0^t \mathrm{t}.\left|\mathrm{e}\left(\mathrm{t}\right)\right| \mathrm{dt}, \quad \mathrm{ITSE} = \int_0^t \mathrm{t}.\mathrm{e}^2\left(\mathrm{t}\right) \mathrm{dt} \tag{54}$$

4. Simulation results

The validity of the presented WECS modeling and the effectiveness of the proposed control strategy applied to MPPT are evaluated using *MATLAB/Simulink* software. The parameters for the turbine and DFIG are provided in *Table 2* and *Table 3*, respectively [51].

4.1 Test1: mechanical characteristics of MPPT algorithms

This test analyzes the performance of an MPPT algorithm under dynamic wind speed conditions. *Figure 11* presents simulation results examining C_P and TSR of a WT over time under varying wind speeds (random and step changes, shown in *Figure 11(a-1) and (a-2)*).

The power coefficient *(C_p)* indicates the energy conversion efficiency of a WT. The maximum value is achieved at a blade pitch angle β and an optimal tip speed ratio λ_{opt} (*Figure 11(1)*), corresponding to the MPPT condition [52]. Since C_p depends nonlinearly on both *TSR* and β [53], its behavior varies accordingly (*Figure 11(3)*). *Figure 11(b-1) and (b-2)* show C_p over time, consistently reaching $C_{p\text{-}max} = 0.48$ despite variations in wind speed [54,55]. *Figure 11(c-1) and (c-2)* illustrate how TSR varies over time under changing wind speeds. *Figure 11(2)* presents a 3D plot of C_p versus TSR and β, indicating that the peak C_p occurs at $\lambda_{obt} = 8.1$ and $\beta = 0°$ [19, 33], though this may not be optimal under all conditions. As shown theoretically in *Figure 11(1)*, aerodynamic limitations cap the efficiency, with the Betz limit setting a maximum $C_p = (16/27) \approx 0.59$. The MPP varies depending on β; each blade pitch angle corresponds to an optimal TSR at which C_p is maximized, highlighting a trade-off between pitch and efficiency. While lower pitch angles can produce higher C_p at specific *TSR* values, they may be less adaptable under changing conditions. Thus, β selection should reflect the turbine's operational environment. The red circle marks a region of high efficiency, though not necessarily the absolute MPP. *Figure 12* illustrates simulation results showing how rotational speed, aerodynamic torque, and power output relate—underscoring the need to optimize for peak efficiency.

The power versus rotational speed curve at various wind speeds shows a consistent parabolic shape, similar to the torque curve (*Figure 12*, right). Both power and torque increase with rotational speed up to a peak, indicating the optimal operational speed for each wind condition. The red circles mark these maximum values, where the turbine extracts substantial energy. *Figure 12* (left curve) also identifies three operating modes: *sub-synchronous* (below optimal speed with high torque but poor energy conversion), *synchronous* (at peak power and maximum efficiency), and *super-synchronous* (above optimal speed with reduced torque and efficiency). This highlights the importance of maintaining operation within the optimal speed range for efficient power generation.

4.2 Test2: Performance of MPPT Algorithm

The objective of the test is to evaluate the effectiveness of various MPPT algorithms, considering both scenarios with/without wind speed control. The aim is to ascertain the precision,

efficiency, and cost-effectiveness of each algorithm. *Figure13* illustrates the simulation outcomes for generator speed and electromagnetic torque, distinguishing between cases with (depicted by blue line) and without (depicted by red line) wind speed.

The simulation results in *Figure 13* show that MPPT with wind speed control (blue line) is more accurate and efficient than MPPT without it (red line), leading to increased power generation and better overall system efficiency. However, MPPT without wind speed control offers the advantages of simplicity and lower implementation costs, relying on continuous adjustments of the WTs operating point for MPPT. In the generator speed curve, the speed increases rapidly in super-synchronous mode (above the synchronous-speed of 1500 rpm, indicated by the red dashed line) when wind speed is measured, reaching a peak of about 2045 rpm at 0.35 second. Conversely, it decreases significantly to a minimum of 340 rpm at 0.75 seconds, entering sub-synchronous mode (below the synchronous-speed). *Table 4* highlights the clear advantages of MPPT with Wind Speed control. Here, the generator operates optimally, with high accuracy and efficiency, leading to superior system performance. Despite the associated higher costs, this approach stands out for its superior performance. Conversely, MPPT without wind speed control may exhibit suboptimal generator operation and moderate performance metrics, but its appeal lies in its simplicity and lower implementation costs, presenting a viable and economical alternative. In essence, the decision between these scenarios entails a careful balancing act between performance metrics and cost considerations.

4.3. Test 3: MPPT's Influence on Mechanical Power Output

To assess the impact of MPPT on mechanical power output, theoretical results are presented, and their accuracy is verified through simulation *(Figure14).* This study aims to evaluate how MPPT algorithms affect the efficiency, stability, and overall performance of WT in generating mechanical power. To understand the relationship between mechanical power and wind speed, the following formula is provided [54]:

$$\begin{aligned} &if: && v < v_{\min} && P_t(v) = 0 \\ &if: && v_{\min} < v < v_B && P_t(v) = \frac{1}{2}\rho.\pi.R^2.v^3.C_p\left(\lambda_{opt}, \beta\right) \\ &if: && v_B < v < v_C && P_t(v) = \frac{1}{2}\rho.\pi.R^2.v^3.C_{p\_\max} \end{aligned} \tag{55}$$

$$if: \quad v_C < v < v_n \qquad P_t(v) = \frac{1}{2}\rho.\pi.R^2.v^3.C_p\left(\lambda_{opt}, \beta\right)$$

$$if: \quad v_n < v < v_{\max} \qquad P_t(v) = P_{t\_\max}$$

In WECS, the turbine output power versus wind speed relationship is typically categorized into four distinct regions (*Figure14* on the right) [19,38,54].

- ***Phase 1 (before point A)****:* When the wind speed is below the cut-in speed, the wind system is not connected to the electrical grid but maintains a minimum rotor rotation speed by adjusting the pitch angle before reaching the cut-in wind speed (point A). In this phase, the system operates in standby mode, awaiting an increase in wind speed.
- ***Phase 2 (A-B)****:* When the wind speed exceeds the cut-in speed, the wind system is connected to the electrical grid, and the mechanical power increases with the wind speed. However, the rotor rotation speed remains at a minimum because the wind speed is still low. Consequently, the *Cp* is not at its maximum value. In this phase, the pitch angle is controlled at zero.
- ***Phase 3 (B-C)****:* The MPPT is achieved in this phase by adjusting the rotor rotation speed based on the variation in wind speed to maintain the optimal speed ratio λ opt. This ensures obtaining the $C_{p\text{-}max}$. The rotor rotation speed varies proportionally with the wind speed.
- ***Phase 4 (C-D)****:* At point C, the rotor speed reaches the rated value. Subsequently, this speed is controlled to its rated value and kept constant to avoid mechanical disturbances and noise in the WT. Therefore, λ is not at the optimal value, and the C_p is lower than in phase (B-C). The WT maintains the optimal pitch angle until the mechanical power reaches the rated value.
- ***Phase 5 (D-E)****:* The wind speed is significant, and the WT's mechanical power output is controlled to the rated value to prevent over current in the power converters and overload in the entire drive train by adjusting the blade pitch angle.
- ***Phase 6 (E-F)****:* Beyond a permissible maximum speed, energy production is halted by (placing the wind turbine in $\beta=0$) to prevent deterioration of the wind turbine and the production system.

To confirm the validity of the previously analyzed theoretical results, simulation results from the *MATLAB/Simulink* environment (*Figure14 on the left*) were presented, showing how the power

output of a WT varies with wind speed. Both curves demonstrate a similar trend of increasing power output with increasing wind speed. Wind turbines operate in four main regions based on wind speed. In ***Region I*** (very low wind speeds below 3 m/s), the turbine blades cannot overcome inertia, resulting in zero power output. In ***Region II*** (low wind speeds 3 m/s to 7 m/s), the wind is strong enough to spin the turbine but generates minimal power, increasing slowly with wind speed. ***Region III*** (medium wind speeds 7 m/s to 12 m/s) is the optimal range for power generation, where the turbine spins rapidly, and power output increases significantly, known as the MPPT region. *Region IV* (high wind speeds above 12 m/s) poses a risk of turbine damage, so the blades angle to shed wind, reducing power output in the cut-out region, determined by the cut-out speed.

4.4 Test 4: Performance Evaluation of VGSTA-SMC-MPPT Algorithm

This test presents a comparative performance analysis of three control algorithms for WTs operating under variable wind speeds. The simulation results (*Figure 15*) evaluate the turbine, gearbox, and electromagnetic torque to assess the VGSTA-SMC algorithm's effectiveness in response speed and torque management.

The curves illustrate how turbine torque varies over time. The *PI* controller regulates turbine torque to ensure stability and optimize power generation, adjusting to changing wind conditions. Meanwhile, *TO-SMC* enhances performance by improving the convergence rate, ensuring higher accuracy in tracking the desired torque, and mitigating the chattering effects commonly associated with lower-order-SMC strategies. This adjustment and responsiveness are reflected in its torque curve. On the other hand, *VGSTA-SMC*, known for its robustness, effectively handles nonlinearities and disturbances. As observed in its turbine torque curve under varying wind speeds (top left of *Figure 15*), *VGSTA-SMC* demonstrates a smoother torque curve and closely tracks the desired output due to its faster adaptation to changing wind conditions. These results in more consistent power generation compared to the *PI* controller and *TO-SMC*. The upper-right curve depicts the gearbox torque, which closely resembles the aerodynamic torque curve but with a lower amplitude. Therefore, the gearbox torque can be considered a representation of the aerodynamic torque, and the following relationship can be written: $T_g = T_t / G$ The curve showed in the bottom of *Figure 15* represents the electromagnetic torque output from the turbine generator (DFIG), which converts mechanical torque from the blades into electrical power. Similar to the turbine torque curve, the PI controller causes more fluctuations and ripples in electromagnetic torque

during wind speed changes. In contrast, *TO-SMC* and *VGSTA-SMC* controls produce smoother torque curves, which potentially lead to more consistent power generation.

Table 5 summarizes these findings. However, the proposed control unit also exhibits certain weaknesses, as identified through curve analysis. These weaknesses include the need for careful parameter tuning to achieve optimal performance, which can be time-consuming and require expertise in control theory. Additionally, compared to PI control, VGSTA-SMC may be more complex to implement due to its non-linear nature. This complexity can increase computational requirements, making it less suitable for resource-constrained systems. Furthermore, *VGSTA-SMC* is sensitive to the initial conditions of the system. If not selected carefully, these conditions may cause the system to fail to converge to the desired sliding surface, a limitation also observed with *TO-SMC*.

4.5 Test 5: Performance Evaluation of the Proposed Control Strategy for DFIG Under Variable Parameters

In this test, the parameters of the DFIG were deliberately altered by reducing the values of both the stator and rotor inductance by 10% of their rated values. This modification was implemented to assess the effectiveness and performance of the VGSTA-SMC strategy applied to the RSC. The proposed strategy's performance was evaluated in comparison to the *TO-SMC* and *PI* control methods. The simulation results, illustrating the active and reactive power responses, are depicted in *Figure 16*.

Simulation results confirm that the VGSTA-SMC strategy effectively tracks reference signals and maintains strong performance despite parameter variations in the DFIG. In contrast, the PI controller shows significant performance degradation, as seen in the distorted active and reactive power curves in *Figure 16*. Compared to TO-SMC, VGSTA-SMC displays reduced oscillations, addresses conventional method limitations, minimizes chattering, and ensures smoother control with finite-time convergence—without requiring higher-order sliding surface derivatives. Both VGSTA-SMC and TO-SMC outperform the PI controller, with VGSTA-SMC achieving the lowest IAE and ISE values (*Table 6*), indicating higher precision. While TO-SMC offers smoother responses and better disturbance rejection (lower ITAE and ITSE), VGSTA-SMC

remains the most robust and efficient method. *Table 7* further compares this proposed technique with other recent control methods, reinforcing its effectiveness.

The proposed VGSTA-SMC control strategy offers a robust solution for improving the performance of DFIG-WT. It enhances stability and efficiency under varying wind conditions by effectively handling disturbances and wind speed fluctuations. Compared to traditional PI controllers, VGSTA-SMC reduces chattering and offers faster dynamic responses. It enables accurate MPP tracking, boosting energy capture. The strategy also improves the turbine's ability to deal with system uncertainties. However, its complexity and higher implementation cost may limit its applicability in cost-sensitive scenarios. Additionally, its performance depends on factors like pitch angle control and TSR, which may not always be optimal. While effective, VGSTA-SMC requires further refinement to simplify implementation and enhance adaptability. Future research should focus on optimizing control parameters and reducing system complexity.

Conclusion

This paper proposes a robust control strategy for Maximum Power Point Tracking (MPPT) in DFIG wind turbines using the Variable Gain Super Twisting Sliding Mode Control (VGSTA-SMC) method. This approach significantly enhances energy conversion efficiency by enabling effective power extraction under variable wind profiles. Compared to TO-SMC and PI control, VGSTA-SMC offers faster adaptation to changing wind speeds—crucial for maintaining optimal turbine performance. The application of VGSTA-SMC at the MPPT level improves the handling of uncertainties and disturbances in the WT system. Simulation results validate its effectiveness in reducing chattering and managing external disturbances more efficiently than TO-SMC methods, demonstrating VGSTA-SMC’s advantages in enhancing DFIG performance under varying wind conditions.

Nevertheless, VGSTA-SMC faces certain challenges, such as sensitivity to initial conditions, limited adaptability, and relatively high control effort, which can lead to increased energy consumption and potential wear on control components. To overcome these drawbacks, future research should focus on enhancing robustness and adaptability through hybrid control techniques—such as combining VGSTA-SMC with Fuzzy-Logic, Neural Networks, or Integral-Backstepping. Additionally, the use of optimization algorithms like Grey Wolf Optimization (GWO), can fine-tune control gains for improved performance. Further advancements may include

integrating multilevel converters to enhance power quality, as well as exploring advanced converter topologies and fault-tolerant designs with optimized LC/LCL filters for better grid compliance. Experimental validation is essential to confirm practical feasibility. Moreover, combining wind systems with other renewable sources (e.g., solar, storage) and leveraging intelligent optimization strategies can contribute to cost-effective, stable, and efficient renewable energy generation under diverse operating conditions.

Nomenclature

A- LIST OF ACRONYMS

DFIG	*Double fed induction generator*
WT	*Wind Turbine*
IEA	*International Energy Agency*
C&I	*Construction and Installation*
O&M	*Operation and Maintenance*
GWEC	*Global Wind Energy Council*
OT	*Optimal Torque*
HCS	*Hill ClimbingSearch*
U-P	*Voltage-Power*
IAE	*Integral of Absolute Error*
ISE	*Integral of SquaredError*
ITAE	*Integral Time AbsoluteError*
ITSE	*Integral Time Square Error*
IFOC	*Indirect Field-Oriented Control*
RSC	*Rotor-Side Converter*
GSC	*Grid-Side Converter*
WECS	*Wind Energy Conversion System*
WES	*Wind Energy System*
MPPT	*Maximum power point tracking*
TSR	*Tip Speed Ratio*
THD	*Total HarmonicDistortion*
PI	*ProportionalIntegral*
SMC	*Sliding Mode Control*
STA	*Super TwistingAlgorithm*
ANNC	*Artificial Neural Network Controller*
FOPI	*Fractional-Order PI Controller*
FOSMC	*Fractional Order Sliding Mode Controller*
DSC-RBF-NN	*Direct speed Control radial basis function neural network*
AFTISMC	*Adaptive fixed-time integral sliding mode control*
OTC	*Optimal Torque Control*
CRONE	*French abbreviation : Commande Robuste d'Ordre Non Entier*
SOSMC	*Second order sliding mode controller*
TO-SMC	*Third order sliding mode controller*
VGSTA	*Variable Gain Super Twisting Algorithm*
GWO	*Grey Wolf Optimization*

B- LIST OF SYMBOLS

$V_{sd} and V_{sq}$	(V)	*Stator direct and quadrature (or transversal) voltage components*
$V_{rd} and V_{rq}$	(V)	*Rotor direct and quadrature (or transversal) voltage components*
$\phi_{sd} and \phi_{sq}$	(Wb)	*Stator direct and quadrature (or transversal) flux components.*

$\phi_{rd} and \phi_{rq}$	(Wb)	*Rotor direct and quadrature (or transversal) flux components.*
$\omega_s and \omega_r$	(rad/s)	*Stator and rotor pulsations*
$R_s and\ R_r$	(Ω)	*Stator and rotor Resistance*
$L_s and\ L_r$	(H)	*Stator and rotor inductance*
M	(H)	*Magnetizing (mutual) inductance.*
$I_{sd} and\, I_{sq}$	(A)	*Stator direct and quadrature (or transversal) current components.*
$I_{rd} and\, I_{rq}$	(A)	*Rotor direct and quadrature (or transversal) current components.*
S	$(--)$	*Slip*
T_{em}	$(N.m)$	*Electromagnetic torque*
T_r	$(N.m)$	*Load torque*
Ω_r	(rpm)	*Mechanical speed*
Ω_t	(rpm)	*Wind turbine speed*
f_t	$(\mathrm{N.m.S^{-1}})$	*Viscous friction coefficient*
J	$(\mathrm{Kg.m^2})$	*Total inertia*
$P_s and\, Q_s$	$(\mathrm{W}\ \&\ Var)$	*Stator active and reactive powers*
P_v	(W)	*Wind turbine power*
R	(m)	*Blade radius*
nP	$(--)$	*Number of blades*
P	$(--)$	*Number of Pole pairs*
G	$(--)$	*The gain of the gearbox*
v	(m/s)	*Wind speed*
λ_{opt}	$(--)$	*Optimal Tip speed ratio (TSR).*
ρ	$(\mathrm{Kg.m^3})$	*Air density*
$\beta°$	(deg)	*Pitch angle*
C_p	$(--)$	*Power coefficient*
C_{p-max}	$(--)$	*Maximum power coefficient*

References

[1]. https://globalwindday.org/

[2]. Hossain, M. I. Hamanah, W. M. Alam, M. S, et al. "Fault Ride Through and Intermittency Improvement of Renewable Energy Integrated MMC-HVDC System Employing Flywheel Energy Storage", in IEEE Access, 11, pp. 50528-50546 (2023).

https://doi.org/10.1109/ACCESS.2023.3277968

[3]. Motlagh, S.Z.T. and, Foroud, A. "Flicker source detection including fixed speed windturbines using empirical mode decomposition," Scientia Iranica, 30(15), pp. 1743–1763 (2023). https://doi.org/10.24200/sci.2022.58053.5541

[4]. Qiucheng, M. Dandan, W. Zongji, X. et al. "Exploring spatio-temporal dynamics for enhanced wind turbine condition monitoring," Mechanical Systems and Signal Processing, 223, (2025). https://doi.org/10.1016/j.ymssp.2024.111841

[5]. Motlagh, S.Z.T. and Foroud, A.A. "Investigation of the compliance of offshore wind data with the Weibull distribution function using six different methods," Scientia Iranica, 30(3), pp. 997–1007 (2023). https://doi.org/10.24200/sci.2022.59152.6078

[6]. https://www.iea.org/

[7]. https://gwec.net /

[8]. Benbouhenni, H. Hamza, G. Oproescu, M. et al. "Application of fractional-order synergetic-proportional integral controller based on PSO algorithm to improve the output power of the wind turbine power system," Sci Rep 14, (2024). https://doi.org/10.1038/s41598-024-51156-x

[9]. Yahdou, A. Belhadj Djilali, A. Bounadja, E. et al. "Using neural network super-twisting sliding mode to improve power control of a dual-rotor wind turbine system in normal and unbalanced grid fault modes," International Journal of Circuite Theory and Applications, 52(9), pp. 4323-4347 (2024). https://doi.org/10.1002/cta.3960

[10]. Itouchene, H. Amrane, F. Boudries, Z. et al. "Design of a Robust Controller using Lyapunov Function for DFIG Wind Turbines," 2024 International Conference on Advances in Electrical and Communication Technologies (ICAECOT), Setif, Algeria, pp. 1-5 (2024). https://doi.org/10.1109/ICAECOT62402.2024.10829237.

[11]. Vali, A.A. Hosseini, S.M.H. and Olamaei, J. "Control of doubly-fed induction generator with extended state observer under unbalanced grid conditions," Scientia Iranica, 29(5), pp. 2498-2514 (2022). https://doi.org/10.24200/sci.2020.55054.4054

[12]. Amrane, F. Francois, B. and Chaiba, A. " Hardware Implementation study of Variable Speed Wind-Turbine-DFIG in Stand-alone Mode," 22nd European Conference on Power Electronics and Applications (EPE'20 ECCE Europe), pp.1-8 (2020). https://doi.org/10.23919/EPE20ECCEEurope43536.2020.9215946.

[13]. Yang, Y. and Xie, W. "Speed Control of Doubly-Fed Induction Generator Based on a Improved Reaching Law Integral Sliding Mode Structure," 2023 4th International Conference on Advanced Electrical and Energy Systems (AEES), pp. 264-269 (2023). https://doi.org/10.1109/AEES59800.2023.10469550

[14]. Mahmoud K.A. Mahmoud A.M. and Ahmed A.H., "Advanced Controls for Wind Driven Doubly Fed Induction Generators," CRC Press. Taylor and Francis Group, 1st Edition (2023). https://doi.org/10.1201/9781003440529-1

[15]. Afzal Thoker Z. and Ahmad Lone, S. "Higher order sliding mode reactive power control of a hybrid power system with wind power and parameter uncertainty," Proceedings of the Institution of Mechanical Engineers, 237(5), pp. 888-903 (2022). https://doi.org/10.1177/09596518221138141

[16]. Itouchene, H. Boudries, Z. Amrane, F. et al. "Improving The Dynamic Response and Power Quality in Wind Turbine-DFIG Systems Using The Super Twisting Algorithm," International Conference on Advances in Electrical and Communication Technologies (ICAECOT), Setif, Algeria, pp. 1-5 (2024). https://doi.org/10.1109/ICAECOT62402.2024.10828701.

[17]. Touati, Z. Mahmoud, I. Araújo, R.E. et al. "Fuzzy Super-Twisting Sliding Mode Controller for Switched Reluctance Wind Power Generator in Low-Voltage DC Microgrid Applications,"energies, 17(6), (2024). https://doi.org/10.3390/en17061416.

[18]. Chojaa, H. Derouich, A. Chehaidia, S.E. Othmane et al. "Integral sliding mode control for DFIG based WECS with MPPT based on artificial neural network under a real wind profile," Energy Reports, 7, pp. 4809-4824 (2021). https://doi.org/10.1016/j.egyr.2021.07.066

[19]. Zhang, X. Jia, J. Zheng, L. et al. "Maximum power point tracking algorithms forwind power generation system: Review, comparison and analysis," Energy Sci Eng, 11, pp. 430-444 (2022). https://doi.org/10.1002/ese3.1313

[20]. Gopinath A, Sankar. N, Srimaheswaran.V, et al. "P&O MPPT-based Wind Power Generation Scheme for Telecom Tower Power Supply," IEEE International Conference on Advancements in Power, Communication and Intelligent Systems (APCI), pp. 1-6 (2024). https://doi.org/10.1109/APCI61480.2024.10617416.

[21]. Aamer Bilal, A.A. Ehsan, R. and Nejman, M. et al. "Recurrent neural network for pitch control of variable-speed wind turbine,"Computer & Information Sciences, 107(2), (2024). https://doi.org/10.1177/003685042412431.

[22]. Chhipa, A.A. Kumar, V. Joshi, R.R. et al, "Adaptive Neuro-Fuzzy Inference System-Based Maximum Power Tracking Controller for Variable Speed WECS," Energies, 14(19), pp. 4809-4824 (2021). https://doi.org/10.3390/en14196275.

[23]. Veerendra, A.S. Vasavi Uma maheswari, M. Peddakapu, K. et al. "Enhancement of a Grid-Connected DFIG Wind Turbine System Using Fractional Order PI Controllers," Renewable Energy Focus, 47, (2023). https://doi.org/10.1016/j.ref.2023.100506

[24]. Zhou, Y. Bhowmick, P. Zhang, L. et al. "A model reference adaptive control framework for floating offshore wind turbines with collective and individual blade pitch strategy," Ocean Engineering, 291, (2024). https://doi.org/10.1016/j.oceaneng.2023.116054

[25]. Mebkhouta, T. Golea, A. Boumaraf, R. et al. "A High Robust Optimal Nonlinear Control with MPPT Speed for Wind Energy Conversion System (WECS) Based on Doubly Fed Induction Generator (DFIG)," Periodica Polytechnica Electrical Engineering and Computer Science, 68(1), pp. 1-11 (2024). https://doi.org/10.3311/PPee.22595

[26]. Delavari, H. and Veisi, A. "A new robust nonlinear controller for fractional model of wind turbine based DFIG with a novel disturbance observer," Energy Systems, 15, pp. 827–861 (2024). https://doi.org/10.1007/s12667-023-00566-3.

[27]. Wang, J. and Bo, D. "Adaptive fixed-time sensorless maximum power point tracking control scheme for DFIG wind energy conversion system," International Journal of Electrical Power & Energy Systems, 135, pp. 1-9 (2022). https://doi.org/10.1016/j.ijepes.2021.107424.

[28]. Hosseinabadi, P.A. Pota, H. Mekhilef, S. et al. "Fixed-time observer-based control of DFIG-based wind energy conversion systems for maximum power extraction," International Journal of Electrical Power & Energy Systems, 146, (2023). https://doi.org/10.1016/j.ijepes.2022.108741.

[29]. Ngo, Q.V. Yi, C. and Nguyen, T.T. "The maximum power point tracking based-control system for small-scale wind turbine using fuzzy logic,"International Journal of Electrical and Computer Engineering, 10(4), pp. 3927-3935 (2020). https://doi.org/10.11591/ijece.v10i4.pp3927-3935

[30]. Ítalo, F.S, Fernando L.T, Paula dos, S.V. et al. "Maximum Power Point Tracking Based on The Curve Sweep Method," 14th IEEE International Conference on Industry Applications (INDUSCON), pp. 38-45 (2021). https://doi.org/10.1109/INDUSCON51756.2021.95296677

[31]. Sai, B. S. V. Chatterjee, D. Mekhilef, S. et al. "An SSM-PSO Based MPPT Scheme for Wind Driven DFIG System," in IEEE Access, 10, pp. 78306-78319 (2022) https://doi.org/10.1109/ACCESS.2022.3193998

[32]. Chen, J. Wang, D. Peng, Z. et al. "Adaptive Extended State Observer Based Direct Voltage Sliding Mode Control of Stand-Alone DFIG-DC System," 5th International Conference on Intelligent Autonomous Systems (ICoIAS), pp. 303-308 (2022). https://doi.org/10.1109/ICoIAS56028.2022.9931285.

[33]. Itouchene, H. Amrane, F. Boudries, Z. "Robust Control of DFIG Wind Turbines in Sub/Super-Synchronous Operation Using Integral Backstepping Controller", Journal of Renewable Energies, 1(1), pp. 23–31 (2024). https://doi.org/10.54966/jreen.v1i1.1170.

[34]. Zeghdi, Z. Barazane, L. and Larabi, A. "Improved Backstepping Control of a DFIG based Wind Energy Conversion System using Anti Lion Optimizer Algorithm," Periodica Polytechnic Electrical Engineering and Computer Science, 66(1), pp. 30-38 (2022). https://doi.org/10.3311/PPee.18716.

[35]. Deep, S. Sarkar, A. Ghawat, M. et al. "Estimation of the wind energy potential for coastal locations in India using the Weibull model", Renewable Energy. 161, pp. 319-339 (2020). https://doi.org/10.1016/j.renene.2020.07.054.

[36]. Barzegar-Kalashani, M. Seyedmahmoudian, M. Mekhilef,, S. et al. "Small-scale wind turbine control in high-speed wind conditions: A review," Sustainable Energy Technologies and Assessments, 60, (2023). https://doi.org/10.1016/j.seta.2023.103577.

[37]. Itouchene, H. Boudries, Z. and Amrane, F. "Improved Power Control based Variable Speed Wind-Turbine DFIG under Hard Work Conditions: Application of Sliding Mode Theory", Periodica Polytechnica Electrical Engineering and Computer Science, 68(4), pp. 392–412 (2024). https://doi.org/10.3311/PPee.36760

[38]. Zhen, Z. Yinan, G. Song, Z. et al "Adaptive integral sliding-mode finite-time control with integrated extended state observer for uncertain nonlinear systems," Information Sciences, 667 (2024). https://doi.org/10.1016/j.ins.2024.120456

[39]. Chetouani, E. Errami, Y. Obbadi, A. et al. "Self-adapting PI controller for grid-connected DFIG wind turbines based on recurrent neural network optimization control under unbalanced grid faults," Electric Power Systems Research, 214 (2023). https://doi.org/10.1016/j.epsr.2022.108829.

[40]. Chojaa, H. Derouich, A. Taoussi, M. et al. "An Improved Performance Variable Speed Wind Turbine Driving a Doubly Fed Induction Generator Using Sliding Mode Strategy," IEEE 2nd International Conference on Electronics, Control, Optimization and Computer Science (ICECOCS), ppp.1-8 (2020). https://doi.org/10.1109/ICECOCS50124.2020.9314629

[41]. Jenkins, N. Burton, T. Bossanyi, E. et al. "Wind Energy Handbook 3e", John Wiley & Sons, Ltd (2021). https://doi.org/10.1002/9781119451143

[42]. Yonis, S. Yusupov, Z. Habbal, A. and Toirov, O. "control approach of a grid connected DFIG based wind turbine Using MPPT and PI Controller," Power Engineering and Electrical Engineering, 21(3), pp. 157-170 (2023). https://doi.org/10.15598/aeee.v21i3.5149

[43]. Dekali, Z. Baghli, L. and Boumediene, A. "Improved Super Twisting Based High Order Direct Power Sliding Mode Control of a Connected DFIG Variable Speed Wind Turbine," Periodica

Polytechnic Electrical Engineering and Computer Science, 65(4), pp. 352-372 (2021). https://doi.org/10.3311/PPee.17989

[44]. Elnaghi, B. E. Abdel-Wahab, M. N. Ismaiel, A. M. et al. "Adaptive Fuzzy Logic Controller For Maximum Power Point Tracking of DFIG Wind Turbine," 24th International Middle East Power System Conference (MEPCON), Mansoura, Egypt, pp.1-5 (2023). https://doi.org/10.1109/MEPCON58725.2023.10462263

[45]. Yessef, M. Bossoufi, B. Taoussi, M. et al, "Improving the Maximum Power Extraction from Wind Turbines Using a Second-Generation CRONE Controller," energies, 15(10), pp. 1-23 (2022). https://doi.org/10.3390/en15103644

[46]. Dendouga, A. Dendouga, A. and Essounbouli, N. "High performance of variable-pitch wind system based on a direct matrix converter-fed DFIG using third order sliding mode control," Wind Engineering, 48(3), pp. 325-348 (2024). https://doi.org/ff10.1177/0309524X231199435.

[47]. Gonzalez, T. Moreno, J. A. and Fridman, L. "Variable Gain Super-Twisting Sliding Mode Control," IEEE Transactionson Automatic Control, 57(8), pp. 2100–2105 (2012). https://doi.org/10.1109/TAC.2011.2179878.

[48]. Javad Mirzaei, M. Ghaemi, S. Badamchizadeh, M.A. et al. "Adaptive super-twisting control for leader-following consensus of second-order multi-agent systems based on time-varying gains," ISA Transactions, vol. 140, p. 144-156 (2023). https://doi.org/10.1016/j.isatra.2023.05.023.

[49]. Gao, X. Li, Y. Ren, X. et al "Variable Gain Super-Twisting Sliding Mode Control for Hammerstein System with Bouc-Wen Hysteresis Nonlinearity," Proceedings of the 35th Chinese Control Conference, Chengdu, China, pp. 3369-3372 (2016). https://doi.org/10.1109/ChiCC.2016.7553876.

[50]. Herizi, A. and Rouabhi, R. "Hybrid Control Using Sliding Mode Control with Interval Type-2 Fuzzy Controller of a Doubly Fed Induction Generator for Wind Energy Conversion,"International Journal of Intelligent Engineering & Systems, 15(1), pp. 549-562, (2021). https://doi.org/10.22266/ijies2022.0228.50.

[51]. https://en.wind-turbine-models.com/turbines/1727-vestas-v82-1.5.

[52]. Nouraldin, N.A. Chebaani, M. Számel, L. et al, "Experimental investigation of predictive control for PMSM-based wind turbine generation system," Computers and Electrical Engineering, 119 (2024). https://doi.org/10.1016/j.compeleceng.2024.109554

[53]. Amrane, F. Francois, B. and Chaiba, A. "Experimental investigation of efficient and simple wind-turbine basedon DFIG-direct power control using LCL-filter for stand-alone mode," ISA Transactions, 125, pp. 631-664 (2022). https://doi.org/10.1016/j.isatra.2021.07.008

[54]. Dekali, Z. Baghli, L. and Boumediene, A. "Improved hardware implementation of a TSR based MPPT algorithm for a low cost connected wind turbine emulator under unbalanced wind speeds" Energy, 232 (2021) https://doi.org/10.1016/j.energy.2021.121039

[55]. Nasiri, M. Milimonfared, J. and Fathi, S.H. "Modeling, analysis and comparison of TSR and OTC methods for MPPT and power smoothing in permanent magnet synchronous generator-based wind turbines," Energy Conversion and Management, 86, pp. 892-900 (2014). https://doi.org/10.1016/j.enconman.2014.06.055.

[56]. Slimane, W. Benchouia, M.T. Golea, A. et al. "Second order sliding mode maximum power point tracking of wind turbine systems based on double fed induction generator," Int J Syst Assur Eng Manag, 11, pp. 716-727 (2020). https://doi.org/10.1007/s13198-020-00987-8

[57]. Chen, Q. Wang, L. Sun, Y. et al "Adaptive integral sliding mode MPPT control for wind turbines with fixed-time convergence,"IET Renewable Power Generation, pp. 1-12 (2024). https://doi.org/10.1049/rpg2.12935

[58]. Muñoz-Palomeque, E. Sierra-García, J.E. and Santos, M. "Wind turbine maximum power point tracking control based on unsupervised neural networks"Journal of Computational Design and Engineering, 10, PP.108-121 (2022). https://doi.org/10.1093/jcde/qwac132

ITOUCHENE Hichem was born in Sétif, Algeria. He earned a B.Sc. and a M.Sc. in Electrical Engineering from the University of Sétif in 2017 and 2019, respectively. In 2021, he began his Ph.D. studies in Electrical Engineering at the Faculty of Electrical Engineering, Béjaïa University, Algeria. He is currently affiliated with the Laboratory of Industrial Technology and Information (LTII). His research focuses on robust control techniques applied to grid-connected and standalone wind turbine power systems based on DFIG, and multilevel converters.

AMRANE Fayssal was born in Batna, Algeria. He received his Bachelor's, Master's, Ph.D., and HdR degrees in Electrical Engineering from the University of Setif-1, Algeria, in 2010, 2012, 2018, and 2022, respectively. Currently, he is a member of the LAS laboratory at Setif-1 University and has been serving as an HdR Lecturer Professor since June 1, 2022. His research interests include the nonlinear control of Wind Energy Conversion Systems, particularly using the DFIG, as well as electrical machine drives and control, intelligent control, multilevel converters, matrix MMC converters, and PWM multilevel rectifiers.

BOUDRIES Zoubir was born in Béjaïa, Algeria. He earned his Ph.D. in Electrical Engineering from the Faculty of Electrical Engineering at Béjaïa University, Algeria, in 2013. He has been a full professor of electrical engineering at the same university since 2021. Currently, he is an active member of the Laboratory of Industrial Technology and Information (LTII). His primary research interests include power electronics, nonlinear control systems, and renewable energy technologies.

List of Figure and Table Captions

List of Figure

List of Table

Table.3 DFIG Parameters [51]

Table.4 Comparison of MPPT with/without wind speed control

Table.5 Comparison of MPPT Methods: *VGSTA-SMC,TO-SMC,* and *PI* Controllers:

Table.6 Numerical values of performance criteria for different controllers

Table.7 Comparison between the proposed *VGSTA-SMC* strategy and alternative research endeavors

Figures and Tables

Figure.1

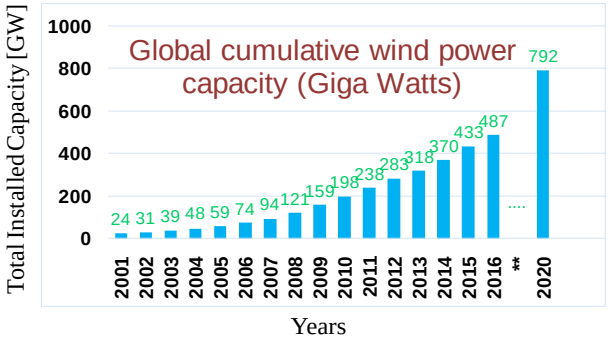

Figure.٢

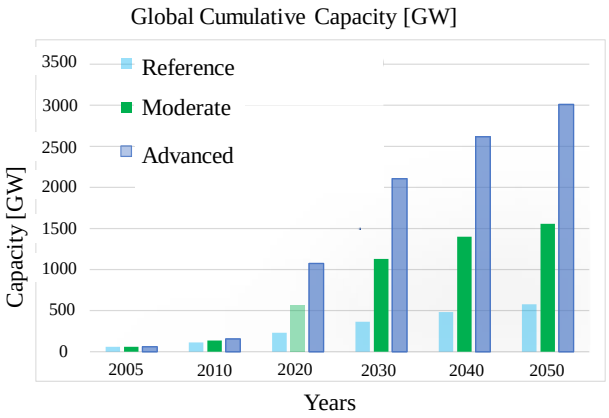

Figure.٣

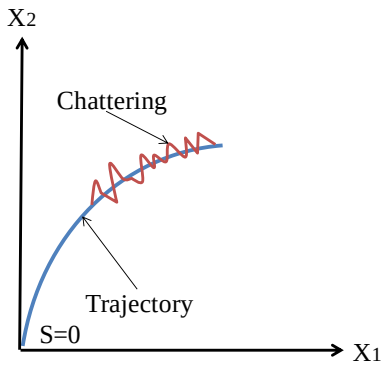

Figure.٤

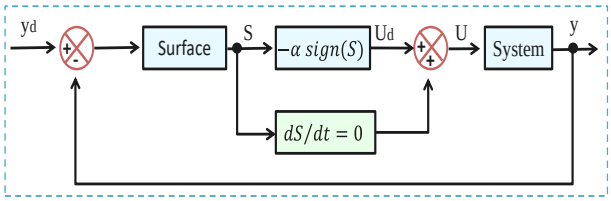

Figure.٥

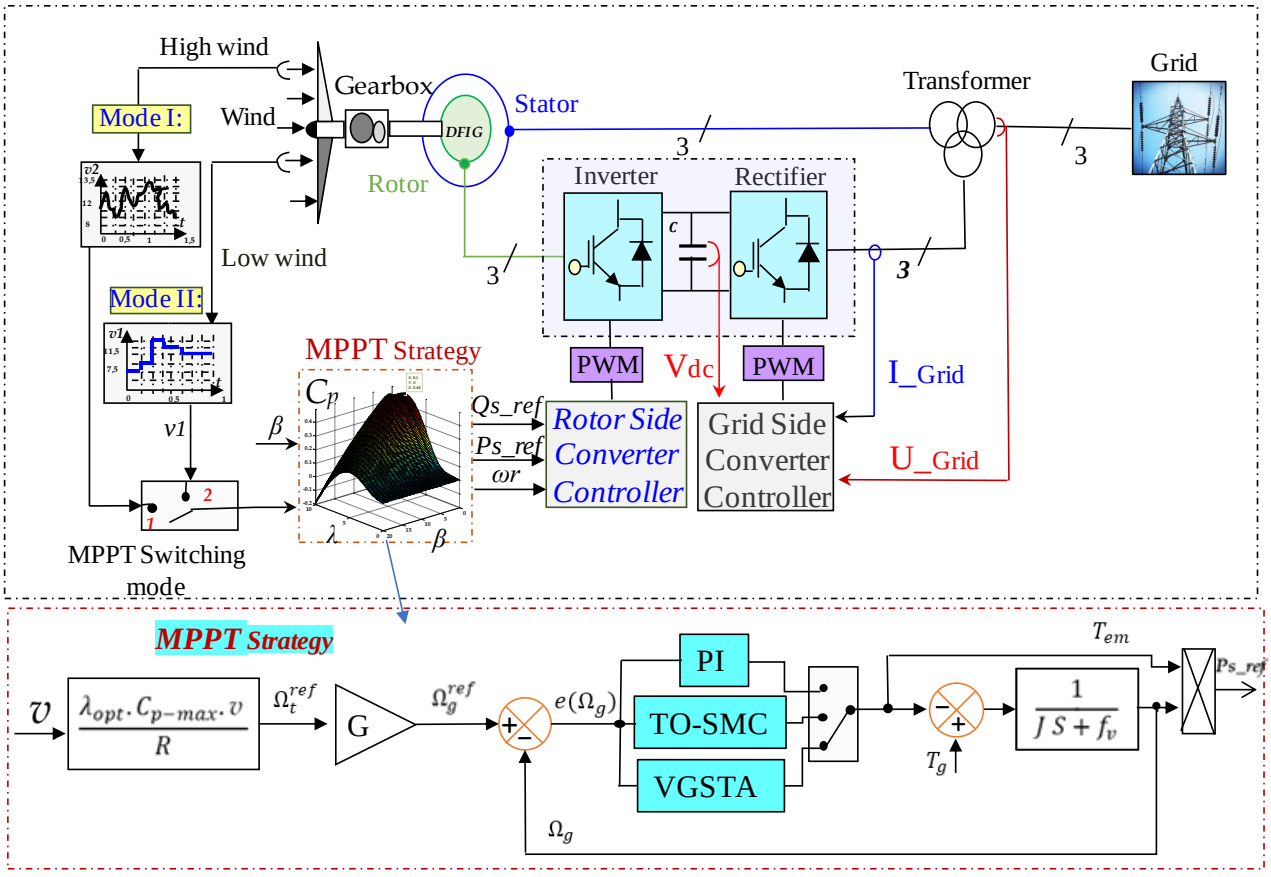

Figure.٦

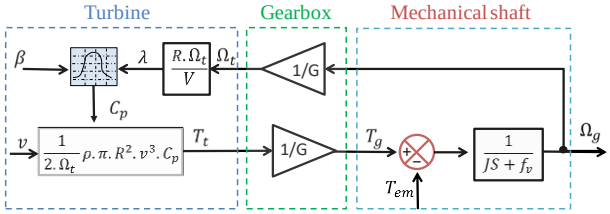

Figure.٧

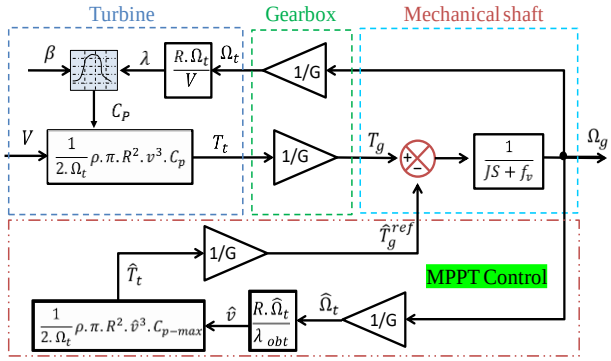

Figure.٨

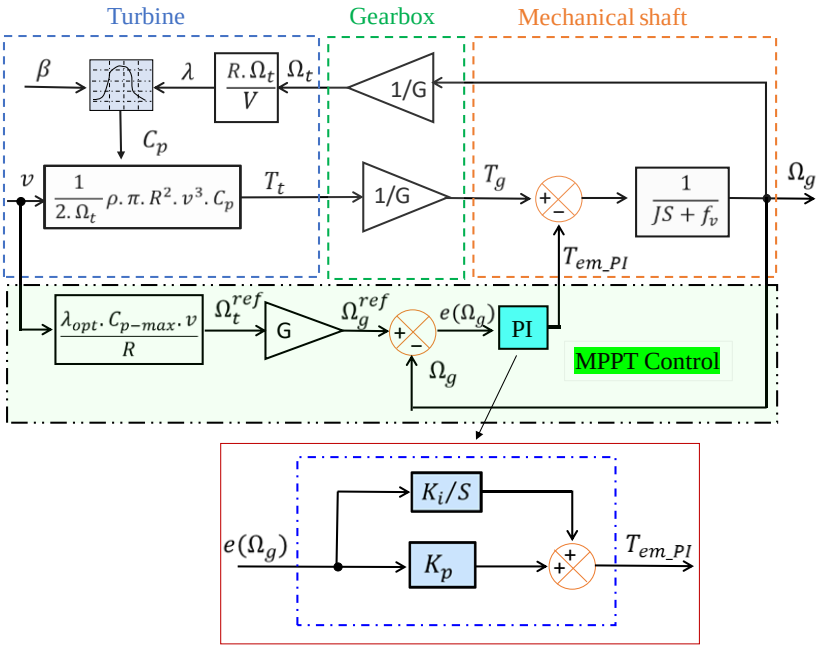

Figure.٩

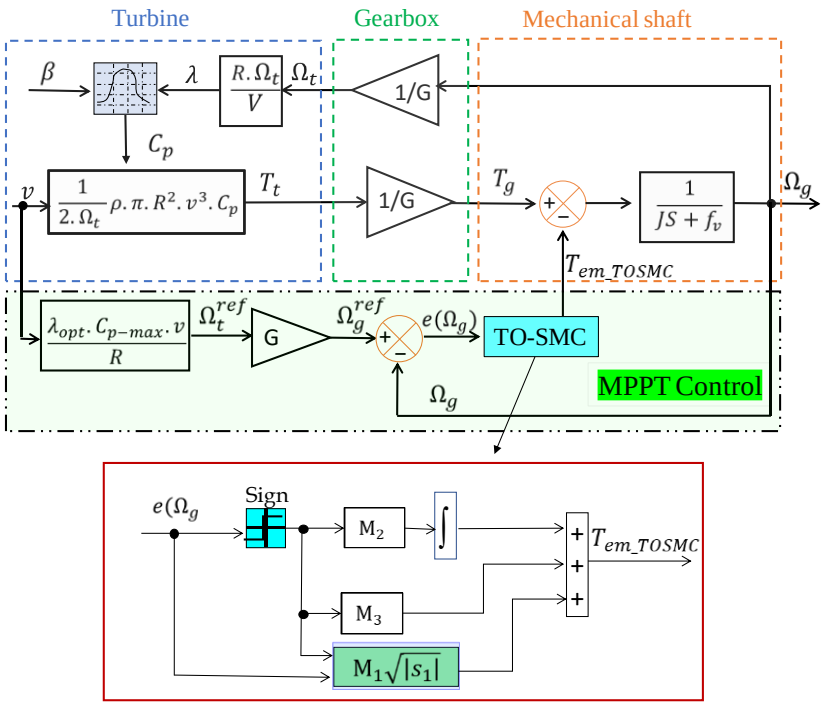

Figure.1

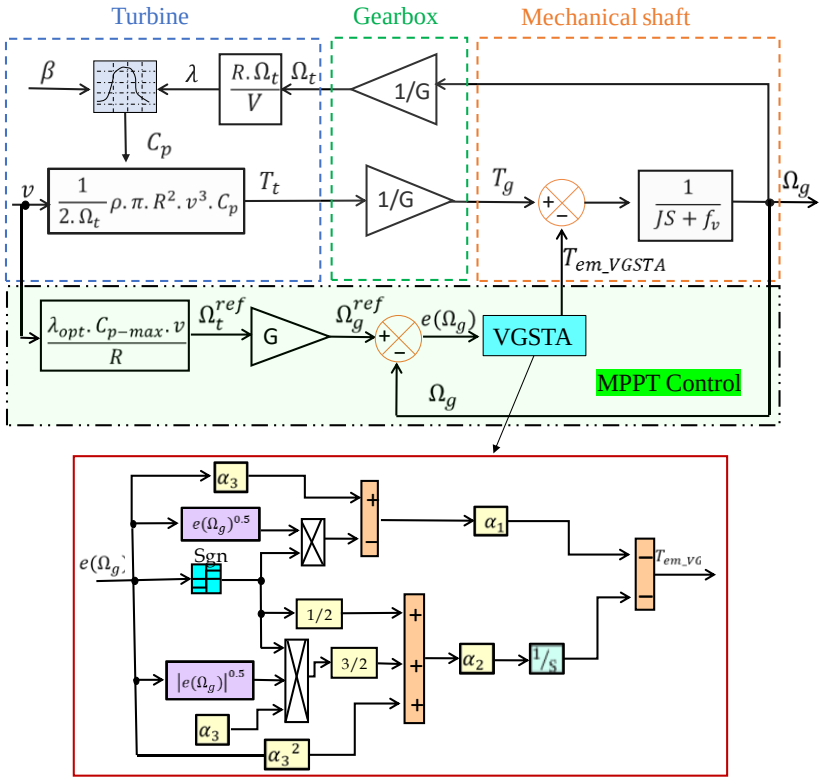

Figure.1

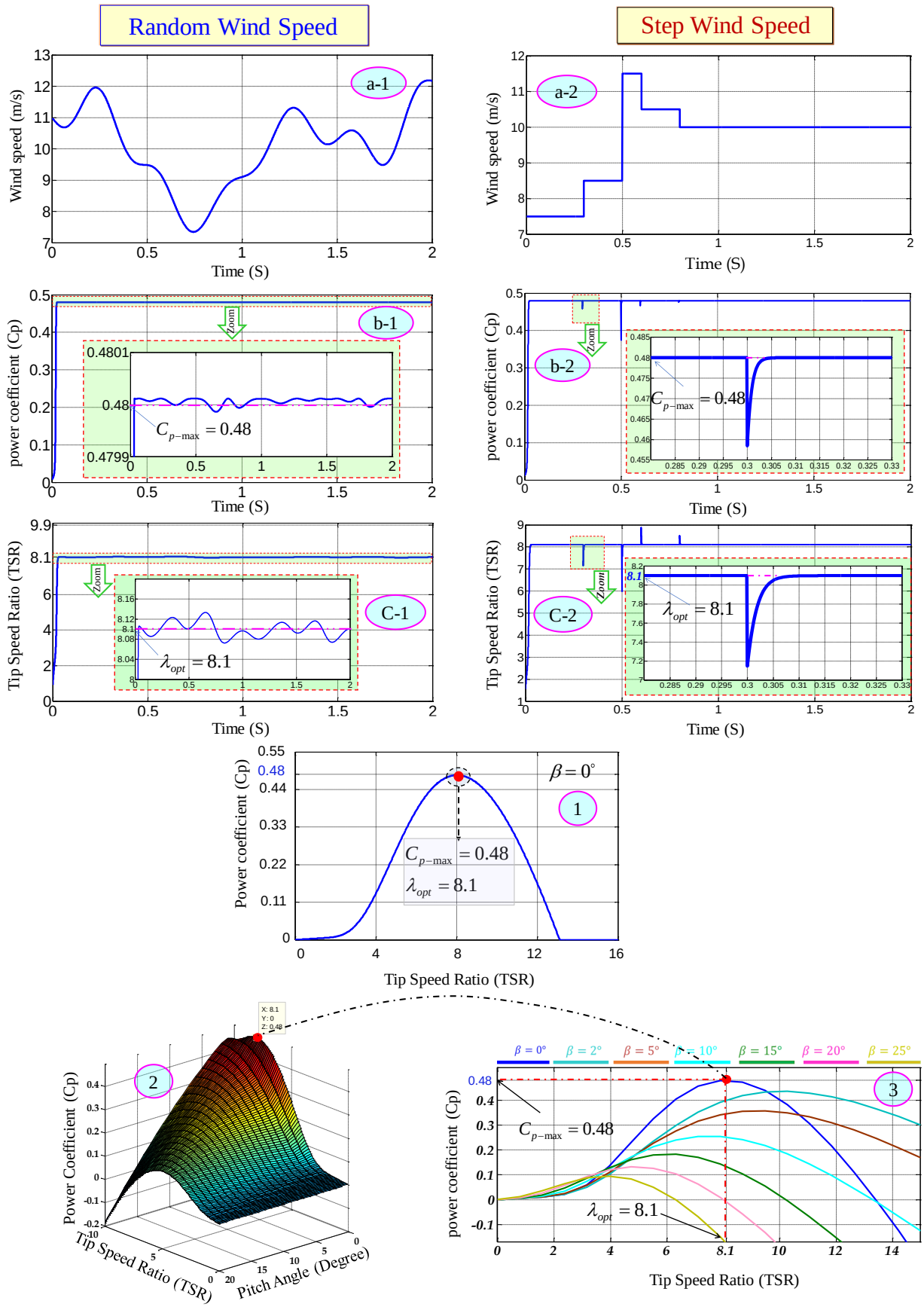
Random Wind Speed
Step Wind Speed
Wind speed (m/s)
Time (S)
a-1
a-2
power coefficient (Cp)
b-1
b-2
Zoom
$C_{p-\max} = 0.48$
Tip Speed Ratio (TSR)
C-1
C-2
$\lambda_{opt} = 8.1$
Power coefficient (Cp)
$\beta = 0°$
1
Tip Speed Ratio (TSR)
Power Coefficient (Cp)
2
Pitch Angle (Degree)
β = 0° β = 2° β = 5° β = 10° β = 15° β = 20° β = 25°
3

Figure.12

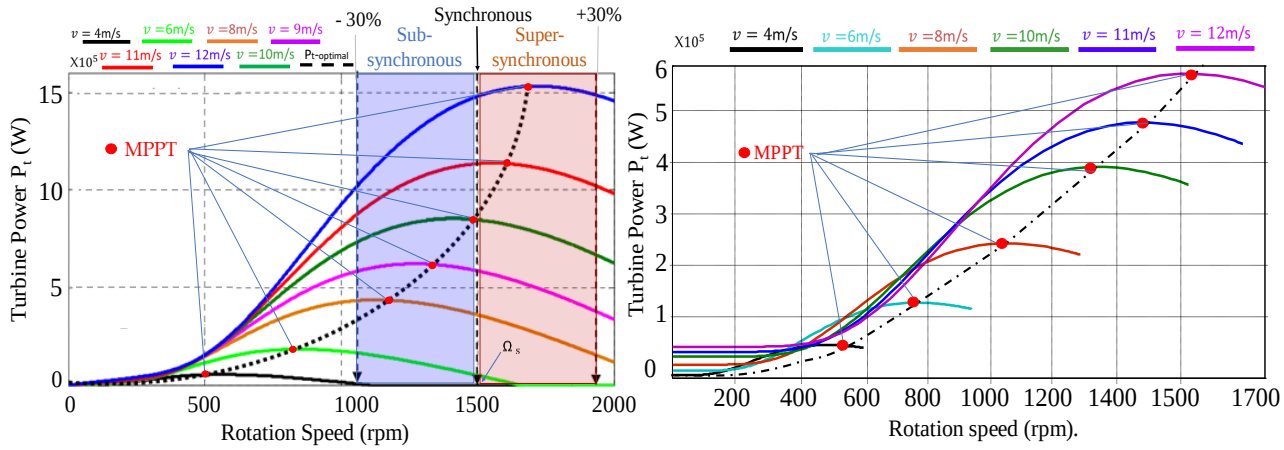

Figure.1٣

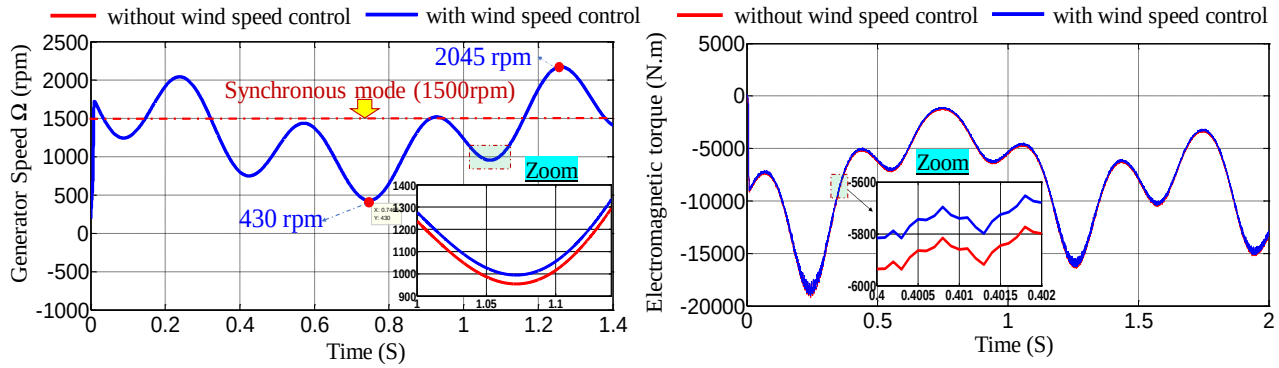

Figure.1٤

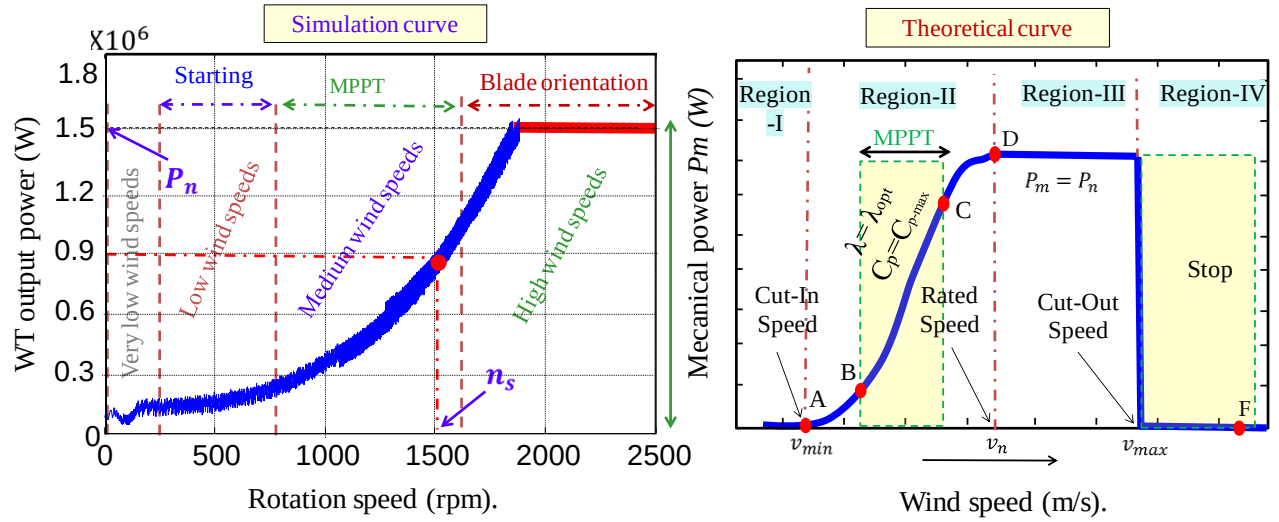

Figure.1

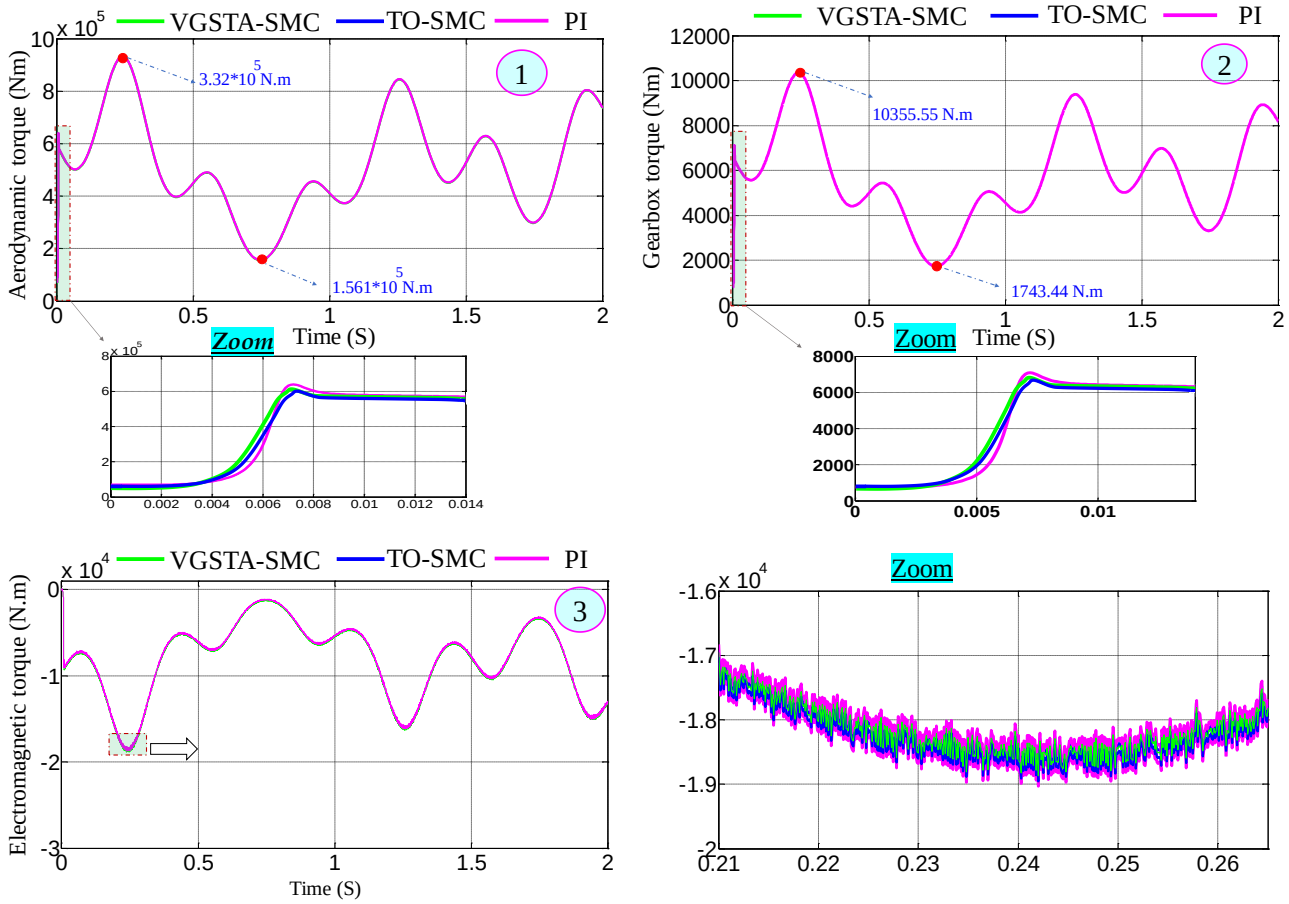

Figure.16

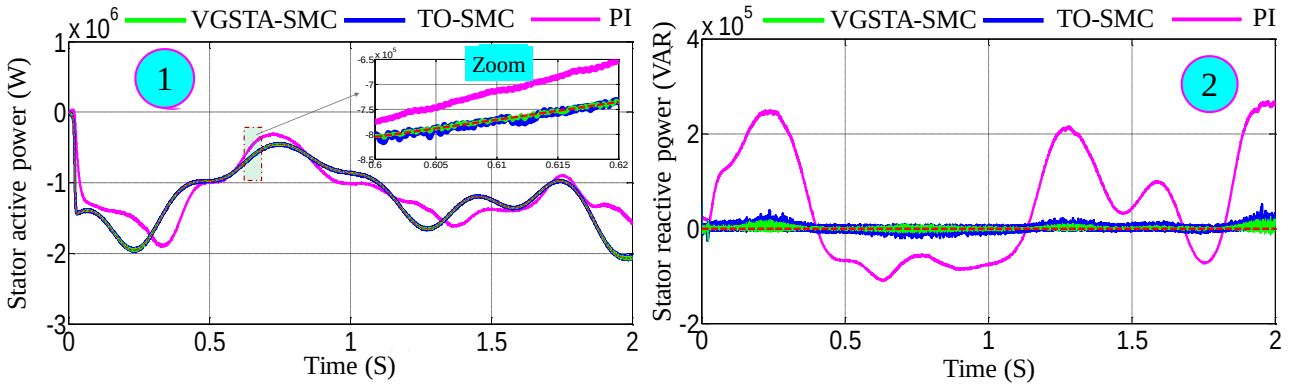

Table.1

Country	*Onshore Wind*		*Offshore Wind*		*total*
	Installations (MW)	***Training Needs (# of technicians)***	***Installations (MW)***	***Training Needs (# of technicians)***	***People***
Australia	7,625	6,624	0	0	6,624
Brazil	16,000	12,308	0	0	13,308
China	300,00	219,622	64,000	29,693	249,315
Colombia	2,250	694	0	0	694
Egypt	3,550	3,017	0	0	3,017
India	21,300	27,653	20	697	28,350
Japan	3,800	3,355	848	1,758	5,113
Kenya	550	574	0	0	574
South Korea	1,000	820	2,299	1,630	2,450
USA	55,000	71,742	11,858	5,751	77,493
Total Ten Contries	**411,075**	**346,409**	**79,025**	**38,529**	**385,938**
Global	**551,475**	**499,481**	**123,018**	**74,694**	**574,175**

Table.٢

R = 35.25 m	Blade radius
np = 3	Number of blades
G = 90	Gearbox ratio
$J = 10^3$ Kg.m^2	Inertia
$f_r = 0.0024$ N.m.S^{-1}	Viscou friction coefficient
V= 12 m/s	Rated wind speed

Table.٣

$P_n = 1.5$ Mw	Rated power
$V_r = 225$ V	Rotor rated voltage
$V_s/U_s = 389/690$ V	Stator rated voltage
$I_n = 1900$ A	Rated current
f = 50Hz	Stator rated frequency
$L_m = 13.5$ mH	Mutual inductance
$L_s = 13.7$ mH	Stator inductance
$L_r = 13.6$ mH	Rotor inductance
$R_s = 12$ mΩ	Stator resistance
$R_r = 21$ mΩ	Rotor resistance
P = 2	Number of pole pairs

Table.٤

	MPPT Strategy	
	With Wind Speed Control	***Without Wind Speed Control***
Speed Generator	Operates at optimal values	May not perates at optimal values
Electromagnetic Torque	Operates at optimal values	May not perates at optimal values
Power Generation	Increased	Decreased
Accuracy	High	Moderate
Response Time	Fast	Slow
Overshoot	Low	Moderate
Efficiency	High	Moderate
Operation Stability	Stable	Unstable
Cost	High	Low
Wind Speed Sensor	Not required	Not required

Table.٥

	MPPT Methods		
	VGSTA-SM Controller	***TO-SM Controller***	***PI Controller***
Adaptability	High	Moderate	Low
Stability	High	Moderate	Moderate
Complexity	High	High	Low
Chattering	Very Low	Low	High
Performance Under Disturbances	Excellent	Good	Moderate
Tuning Difficulty	High	High	Low
Precision	Very High	High	Moderate
Overshoot	Neglected (2%)	Low (10%)	Remarquable (70%)
Respense Time	Fast	Moderate	Low

Table.٦

	MPPT Methods		
	VGSTA-SM Controller	***TO-SM Controller***	***PI Controller***
ITSE (P_s)	$3.955*10^7$	$4.081*10^7$	$11.53*10^7$
ITSE (Q_s)	$3.162*10^7$	$2.58*10^7$	$7.58*10^7$
IAE (P_s)	2549	2561	9465
IAE (Q_s)	2230	2252	8320
ITAE (P_s)	1964	1972	6937
ITAE (Q_s)	1900	1921	7498
ISE (P_s)	$1.153*10^8$	$1.159*10^8$	$3.97*10^8$
ISE (Q_s)	$4.641*10^7$	$4.276*10^7$	$11.17*10^7$

Table.٧

Reference Paper	***MPPT Technique***	***Response Time (s)***	***Static Errors (%)***	***Set-Point Tracking***	***Generator***
[25]	LQR	Fast (--)	Little (--)	Good	DFIG
[45]	CRONE	Fast (0.0012)	Low (0.3)	Good	DFIG
[55]	OTC	Medium (0.02488)	---	Good	PMSG
[56]	SOSMC	Fast (0.002)	---	Good	DFIG
[57]	AFTISMC	---	Moderate (0.0751)	Good	---
[58]	DSC-RBF-NN	Fast (0.004)	---	Good	DFIG
Proposed method	**VGSTA-SMC**	**Fast (0.001)**	**Little (0.4)**	**Very Good**	**DFIG**
(---) No data is available.					